

1.5 μm quantum-dot diode lasers directly grown on CMOS- standard (001) silicon

Si Zhu^{1,a)}, Bei Shi^{1,a)}, Qiang Li¹, and Kei May Lau^{1*}

¹Department of Electronic and Computer Engineering, Hong Kong University of Science and Technology,
Clear Water Bay, Kowloon, Hong Kong

a) B. Shi and S. Zhu contributed equally to this work

* Tel: (852)23587049, Fax: (852) 23581485, Email: EEKMLAU@UST.HK

ACCEPTED MANUSCRIPT

Electrically pumped on-chip C-band lasers would provide additional flexibility for silicon photonics in the design of optoelectronic circuits. III-V quantum dots, benefiting from their superior optical properties and enhanced tolerance to defects, have become the active medium of choice for practical light sources monolithically grown on Si. To fully explore the potentials of integrated lasers for silicon photonics in telecommunication and datacenter, we report the realization of 1.5 μm room-temperature electrically pumped III-V quantum dot lasers epitaxially grown on complementary metal-oxide-semiconductor (CMOS)-standard (001) Si substrates without offset. A threshold current density of 1.6 kA/cm^2 , a total output power exceeding 110 mW and operation up to 80 $^\circ\text{C}$ under pulsed current injection have been achieved. These results arose from applying our well-developed InAs/InAlGaAs/InP QDs on low-defect-density InP-on-Si templates utilizing nano-patterned V-grooved (001) Si and InGaAs/InP dislocation filters. This demonstration marks a major advance for future monolithic photonic integration on a large-area and cost-effective Si platform.

Driven by the low-cost and high-throughput production of silicon-based CMOS infrastructures, silicon photonics (SiPh) is evolving rapidly addressing the growing demands for optical communications¹. The Si-Ge-silica platform has been used for monolithic integration of modulators, filters, (de)multiplexers, splitters and detectors². SiPh products involving these components have already been commercialized^{3,4} in high-performance computing (HPC), interconnects, telecommunications and sensors applications. Very recently, a dense integration of photonics with silicon nanoelectronics on a bulk CMOS Si chip has been announced⁵. Among all these demonstrations, an efficient coherent light source is the only key component remaining elusive for on-chip integration, due to the indirect-bandgap nature of silicon and germanium for efficient lasers⁶. As an alternative to bonding, epitaxial growth of III-V materials on Si stands to

become a competitive solution as it potentially provides a low-cost solution for mass production⁷.

Recent efforts are devoted to perfecting the gain elements and defect engineering in III-V on Si heteroepitaxy.

III-V quantum dots have proven superior optical properties and high tolerance to defects in lasers directly grown on silicon⁸. GaAs-based QD lasers on Si in 1-1.3 μm range have demonstrated excellent performance with diverse designs⁹⁻¹¹. However, to extend the emission wavelength of InAs/(In)GaAs based QDs beyond 1.3 μm has been challenging¹²⁻¹⁴. Specifically, development of QD lasers on Si emitting at 1.55 μm band is important, for low loss transmission in mid/long-haul communications and for compatibility with commercial Erbium Doped Fibre Amplifiers (EDFAs) to enable dense-wavelength division multiplexing (DWDM). Our effort has been devoted to the investigation of 1.55 μm -band emission from InAs QDs embedded in InP-based alloys¹⁵. A few ternary/quaternary alloys lattice-matched to InP are tunable to demonstrate lasing ranging from 1.2 to 2 μm ¹³. We have previously reported the room-temperature (RT) optically-pumped C-band QD laser on CMOS-standard (001) Si^{16,17}. To take a step further toward electrically pumped diode lasers, two major challenges have to be carefully addressed. The first is associated with crystalline defects due to the structural mismatches between III-V materials and Si. Especially for InP, the lattice mismatch with Si is $\sim 8\%$, twice the mismatch between GaAs and Si ($\sim 4\%$). The second issue originates from the complex growth kinetics and the weak driving force for QD formation on InP, which makes them more difficult to grow than InAs/GaAs QDs. In this work, by well addressing these two major challenges, we demonstrate the room-temperature electrically-pumped InAs QD laser on (001) Si operating at the 1.5 μm telecom-band.

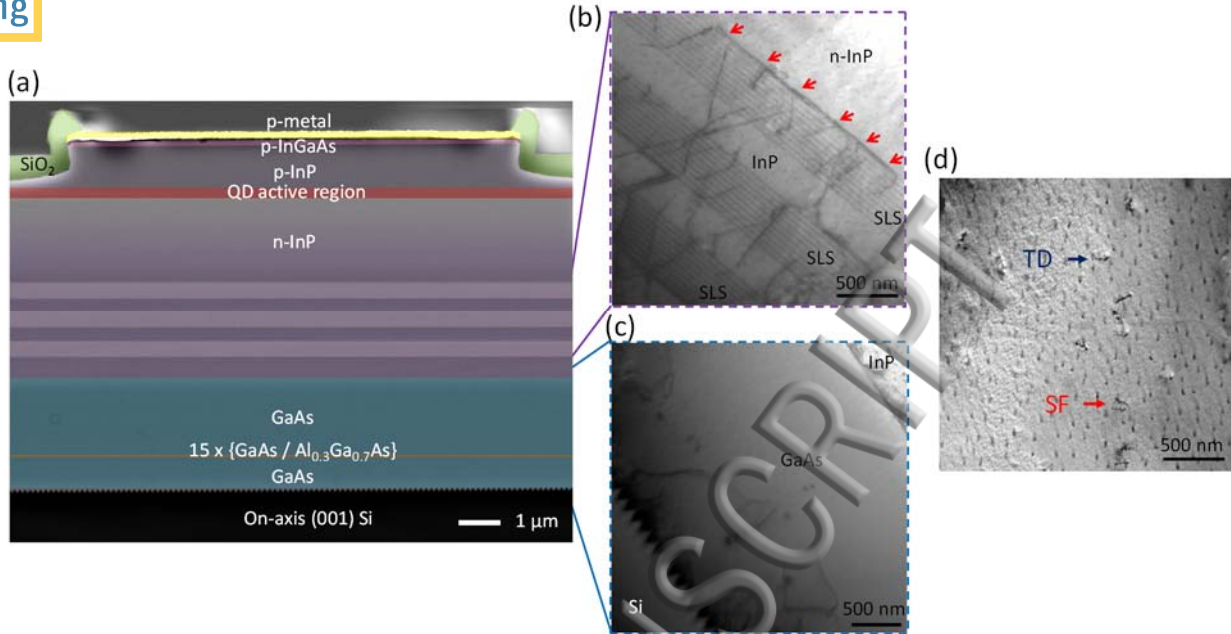


FIG. 1. (a) Color-enhanced cross-sectional SEM image of the whole epitaxial structure. Cross-sectional TEM images of (b) 3 stacks of 10-period InGaAs/InP SLSs with dislocation filtering effects identified by red arrows, (c) 2.2- μm -thick GaAs intermediate buffer on nano-patterned V-grooved on-axis (001) Si substrate, and (d) Plan-view TEM characterization of defect density of the InP buffer on Si.

In contrast to most reported works using 2-6° offcut Si towards (110) planes to prevent the formation of anti-phase boundaries (APBs)^{9,18}, a specially manufactured V-grooved on-axis (001) Si is adopted¹⁹. The employment of (001)-oriented Si or silicon-on-insulator (SOI) wafers eases the integration of photonic and electronic components in CMOS manufacturing infrastructures. The complete epitaxial structure on Si is shown in the cross-sectional scanning electron microscope (SEM) in Fig. 1(a). Growing GaAs on Si V-grooves basically relaxes the misfit strain by the formation of twinned stacking faults (SFs), which are aligned in the {111} nucleation planes and mostly trapped by the Si ridges. The coalesced GaAs with fifteen periods of 5-nm

$\text{In}_{0.5}\text{Ga}_{0.7}\text{As}/5\text{-nm GaAs}$ superlattices (SLs) exhibits a smooth growth front and free of pinholes or APBs. The GaAs buffer on V-grooved Si (Fig. 1(c)) shows a superior crystalline quality. During the growth of InP buffer, threading dislocations (TDs), typically in the order of $10^9\text{-}10^{10}\text{ cm}^{-2}$, are nucleated from the hetero-interface of InP/GaAs. To further deter the dislocations inside the InP layer to propagate, ten periods of 10-nm $\text{In}_{0.6}\text{Ga}_{0.4}\text{As}/30\text{-nm InP}$ strain layer superlattices (SLSs) were inserted to filter the dislocations and repeated for three times, separated by 250 nm high-temperature InP spacer. Detailed growth parameters and characterizations are provided in the [Supplementary](#). The dislocation filtering effect of the SLSs is manifested by the cross-sectional transmission electron microscopy (XTEM) in Fig. 1(b). The Peach-Koehler force, determined by the strain of InGaAs, will repel/guide the dislocations laterally towards the edge of the sample and parallel to the growth plane at the interface of each SLS, resulting in the coalescence and annihilation of dislocations. A low defect density ($1.5\times 10^8\text{ cm}^{-2}$) is characterized by plan-view TEM in Fig. 1(d), one of the lowest reported defect density values for InP film grown on Si substrates by metalorganic chemical vapor deposition (MOCVD)²⁰. The InP template roughness is reduced to below 2 nm over an AFM scanning area of $10 \times 10\ \mu\text{m}^2$, important for subsequent QD epitaxy with reduced inhomogeneity.

With room-temperature photoluminescence (PL), effort has been made to minimize the QDs inhomogeneous broadening for the operation of InP-based QD lasers on Si. By capping the InAs QDs using a double-cap procedure and carefully tuning the thickness of each cap layer²¹, the optimized 5-stack QDs on Si exhibit a multi-modal size distribution with the strongest peak centered at 1512 nm and a narrow linewidth of 61.6 meV (Fig. 2(a)). This PL FWHM is slightly higher than the state-of-art values of QDs on InP substrates^{22,23}. Moreover, additional tuning of the QDs growth parameters led to an over 4 times stronger peak PL intensity and 1.6 times

ing narrower FWHM than the previous batch of QDs²¹. Here, the multi-modal size distribution is attributed to the non-uniformity of QD sizes^{24,25}, rather than the effects of the stacking process, as evidenced by the multi-peak PL spectrum of single layer QDs in Fig. 2(a). Nevertheless, inhomogeneous broadening is still observed when stacking these QDs, as evidenced by the narrower FWHM of 47.2 meV for single layer QDs. More studies on the QD size distribution are carried out in [Supplementary](#). The coherent multi-stack QDs on Si, characterized by atomic force microscopy (AFM) in the inset of Fig. 2(a), present a QD density of $\sim 4.5 \times 10^{10} \text{ cm}^{-2}$. Leveraging the well-developed QDs on high quality InP-on-Si, a diode laser structure containing five layers of InAs/InAlGaAs QDs was grown, showing a smooth surface with root mean square (RMS) value of 1.4 nm and a desirable morphology (Fig. 2(b)).

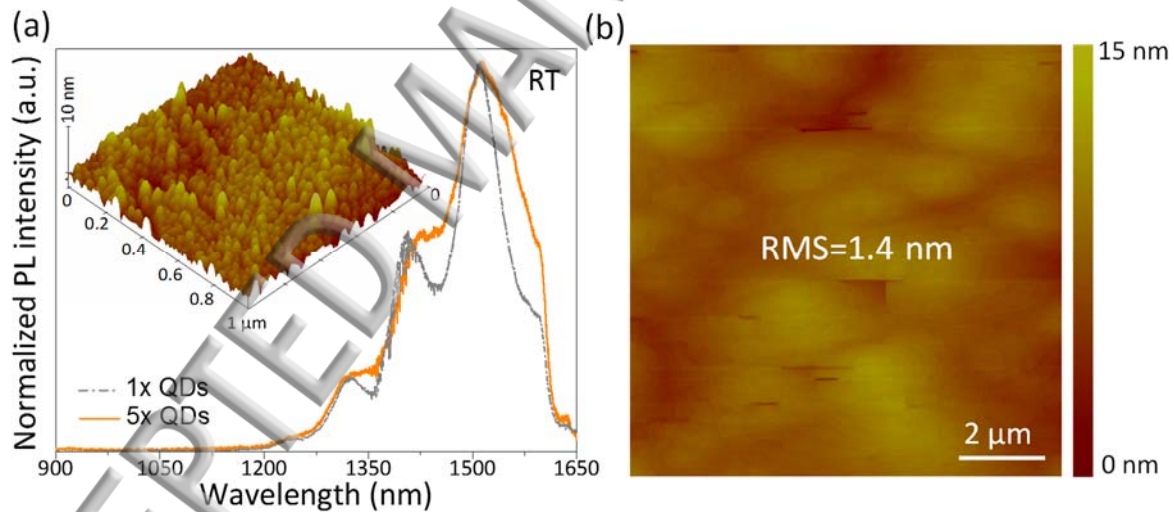


FIG. 2. (a) Normalized room-temperature photoluminescence spectra of 1 and 5 layers of QDs active region grown on Si. Inset shows an AFM image of the top layer QDs with a density of $4.5 \times 10^{10} \text{ cm}^{-2}$. (b) AFM image of the as-grown QD laser on silicon, showing a smooth surface with an RMS value of 1.4 nm.

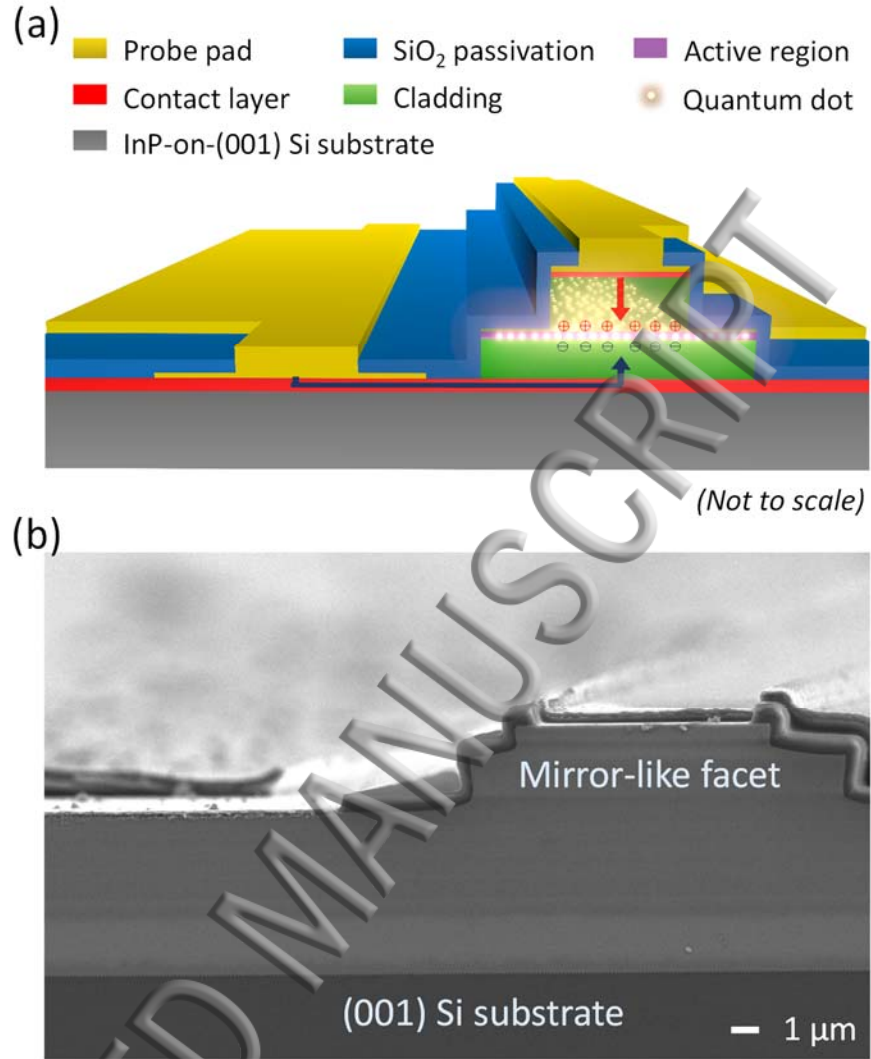


FIG. 3. (a) Schematic of an InAs/InAlGaAs/InP QD laser on a silicon substrate. (b) SEM overview of the complete QD laser on (001) silicon.

With the InAs/InAlGaAs/InP QDs on (001) Si epitaxial laser structure, ridge waveguide edge-emitting lasers was processed by standard photolithography, dry-etch and metallization techniques.

The facets were cleaved and left uncoated. Fig. 3(a) schematically shows the diode laser architecture. The “top-top” contact geometry is designed to bypass the defective III-V/Si interface for efficient electrons and holes injection. Thus, a dry-etch process to expose the n-InP layer needs

careful optimizations for a good n-type contact. Detailed fabrication parameters are provided in [Supplementary](#). An overview SEM image of a completed device with 8 μm waveguide width is presented in [Fig. 3b](#). A very clean and mirror-like facet has been achieved, which is essential for minimized cavity loss.

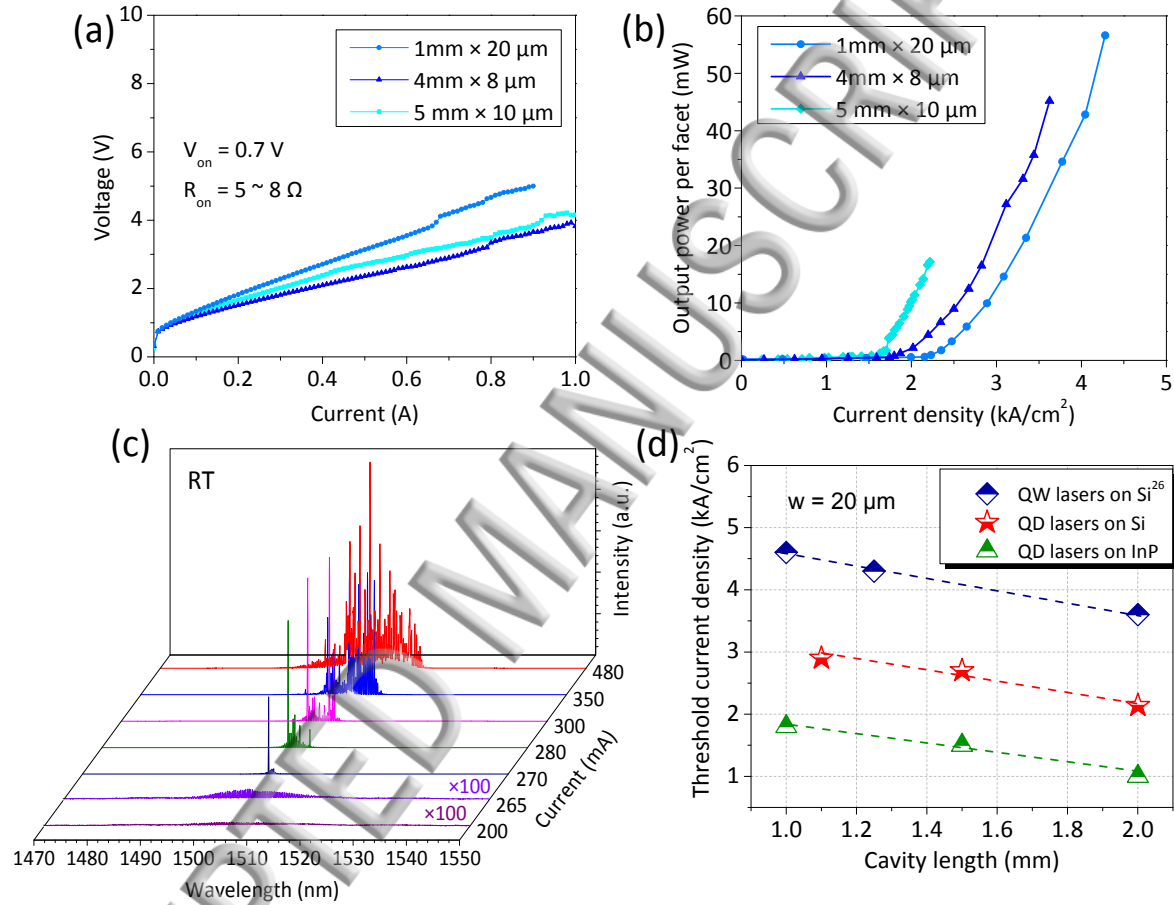


FIG. 4. (a) (b) LIV characteristics for three InAs/InAlGaAs/InP QD lasers grown on (001) Si substrate under pulsed operation at RT. (c) Emission spectra for a 10 $\mu\text{m} \times 1,000\ \mu\text{m}$ device at various injection current. (d) Threshold current density distribution of optimized QD lasers on InP and Si, compared with QW lasers directly grown on (001) Si^{26} at varied cavity lengths (width=20 μm).

Grown laser bars were tested at room-temperature under pulsed current injection. Representative light-current-voltage (LIV) characteristics for three different laser cavity sizes are shown in Figs. 4(a) and 4(b). The turn-on voltage of the QD laser diode on (001) Si is 0.7 V, and as the ridge width becomes narrower, the series resistance rises slightly but all fall in the range of 5-8 Ω . A threshold current density J_{th} of 1.6 kA/cm² (320 A/cm² per QD layer) from a 5 mm \times 10 μ m laser can be extrapolated according to the kink on the L-I curve. No output saturation was observed when the output power reached 57 mW per facet, corresponds to a total output power exceeding 110 mW. Statistical threshold data of all tested devices are presented in Supplementary Fig. S4. The electroluminescence (EL) spectra from one 1 mm \times 10 μ m QD laser on (001) Si at different injection currents are shown in Fig. 4(c). For a fair evaluation of threshold difference between QD lasers grown on (001) Si and native InP substrate, both categories of devices with different cavity widths were subjected to pulsed measurement. It should be pointed out that QD lasers grown on InP can operate under continuous-wave pumping at room-temperature. As shown in Fig. 4(d), the threshold densities of QD lasers on Si is averagely two times higher than those on InP, suggesting further improvement of InP-on-Si templates is needed. Meanwhile, the threshold current densities of QD lasers and our previously reported QW lasers on Si²⁶ with the same configurations are also compared in Fig. 4(d), showing an average threshold reduction of 1.6 times for QD lasers. This result clearly suggests the QDs active medium as a promising candidate for lasers monolithically grown on Si. The lasing wavelength tunability from 1478 nm to 1523 nm in different cavity lengths is demonstrated and discussed in detail in Supplementary.

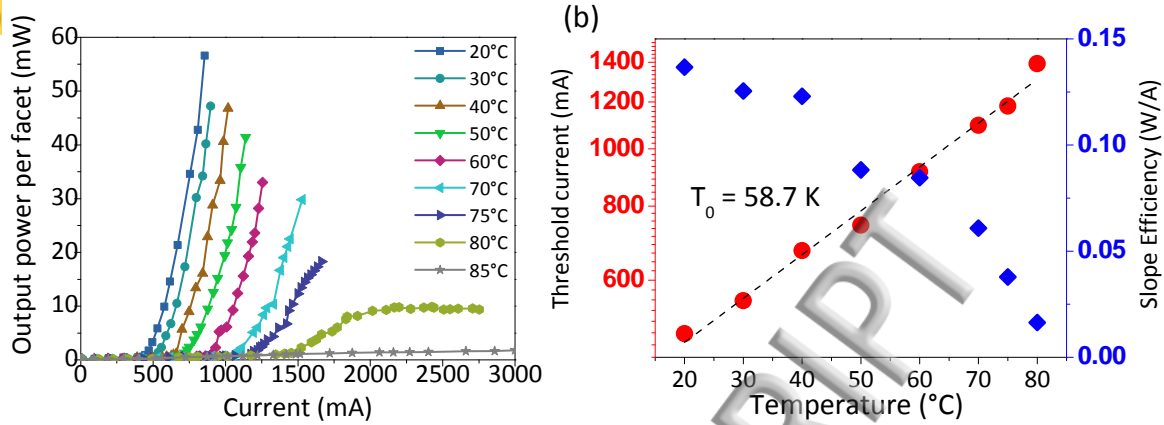


FIG. 5. (a) Light output power versus current for a $20 \mu\text{m} \times 1,000 \mu\text{m}$ device at various temperatures. **(b)** Threshold current and slope efficiency change as a function of temperature. The characteristic temperature is extracted to be 58.7 K.

Temperature-dependent characteristics were studied for these $1.5 \mu\text{m}$ diode lasers grown on (001) Si, as the capability to operate at elevated temperatures is a critical criterion for on-chip lasers. Fig. 5(a) shows a set of LI curves measured from 20°C to 85°C . A slope efficiency droop and obvious power saturation around 10 mW/facet are noted at 80°C . The characteristic temperature T_0 is estimated to be 58.7 K (Fig. 5b), which is a reasonable value for InAs/InAlGaAs/InP QD lasers. The T_0 value is anticipated to be dramatically increased by p-type modulation doping²⁷. To investigate the wavelength stability, which is another superiority expected from QDs, primary lasing wavelengths versus temperature was also measured (Supplementary Fig. S5). An average temperature coefficient $\frac{\Delta\lambda}{\Delta T} = 0.3 \text{ nm/K}$ can be obtained, which is even smaller compared to those QD lasers on InP substrate^{13,28}. The laser performances are not yet on par with GaAs-based $1.3 \mu\text{m}$ QD lasers on Si due to the intrinsic difficulties discussed above. Therefore, on-going work will be first focused towards continuous-wave (CW) operation by adopting the tunnel injection structures,

ing which QDs are separated from an InGaAs QW by the ultrathin InAlGaAs barrier for more efficient carrier injection²⁹. Also, increasing the Indium composition in the InGaAs interlayers to introduce a larger strain field would be beneficial for enhanced dislocation filtering. Additional structures like slotted grating couplers³⁰ can be adopted forcing the light down from the epitaxial laser to the Si waveguide to integrate with the existing SiPh circuits.

In summary, by harnessing nano-patterned V-grooved (001) Si and InGaAs/InP SLS for defect reduction and InAs/InAlGaAs QDs as the gain media, we have realized the 1.5 μm long wavelength QD diode lasers epitaxially grown on CMOS-standard (001) Si. Pulsed operation with a low threshold current density of 1.6 kA/cm^2 , a total output power exceeding 110 mW and lasing up to 80 °C have been demonstrated. More informative comparisons between QD lasers on Si and those on InP as well as QW laser counterparts on Si are conducted, to verify the suitability of QDs in lasers epitaxially grown on Si. Our results indicate that, the large mismatch between InP and Si is no longer a fundamental limitation for monolithically integrating practical lasers and other III-V elements on Si-Ge-silica platform by the heteroepitaxy approach. The technology to grow large-area high-quality InP on Si also offers a possibility to adopt Si as a low-cost scalable substrate and leverage the suite of techniques and processes already commercialized in InP PICs³¹. Furthermore, the utilization of bulk CMOS (001) Si wafers also demonstrate a great stride in the evolution towards monolithic photonic and electronic integration on the silicon-based microelectronics platform with cost-effective solution and abundant supply chain.

Supplementary material

See [supplementary material](#) for detailed growth and fabrication methods and laser characterizations.

Acknowledgements

The authors acknowledge financial support from the Innovation Technology Fund of Hong Kong (No. ITS/273/16FP). The authors would like to thank the Nano-Fabrication Facility and the Material Characterization & Preparation Facility of HKUST, the Suzhou Institute for Nano-tech and Nano-bionics, Chinese Academy of Science for technical support, and SUNY Poly for providing the initial nano-patterned Si substrates.

References

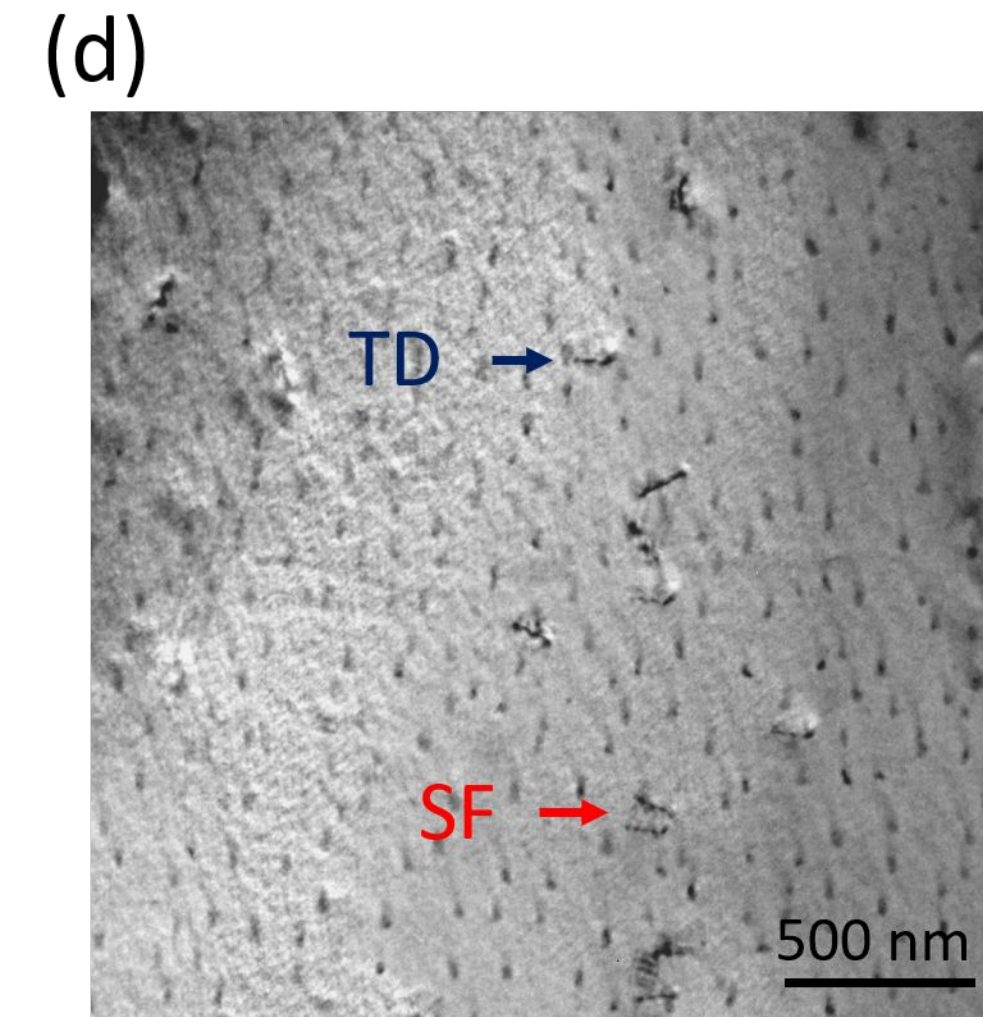
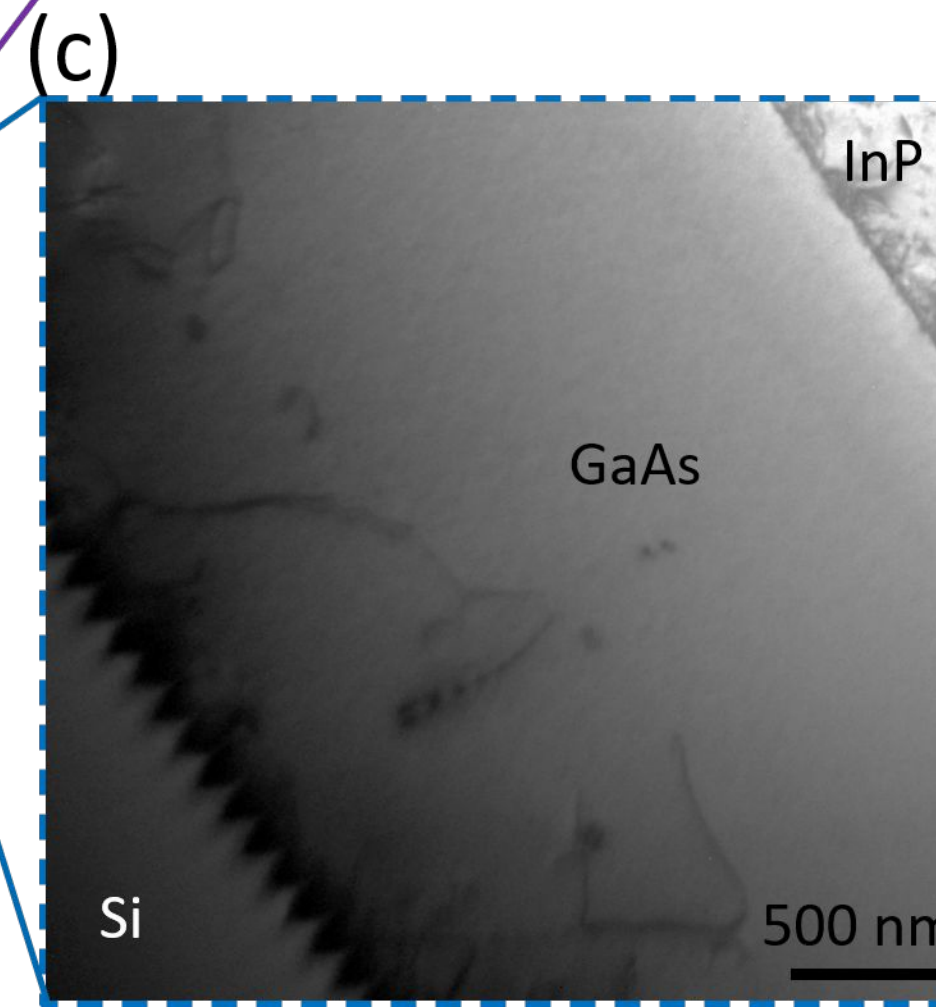
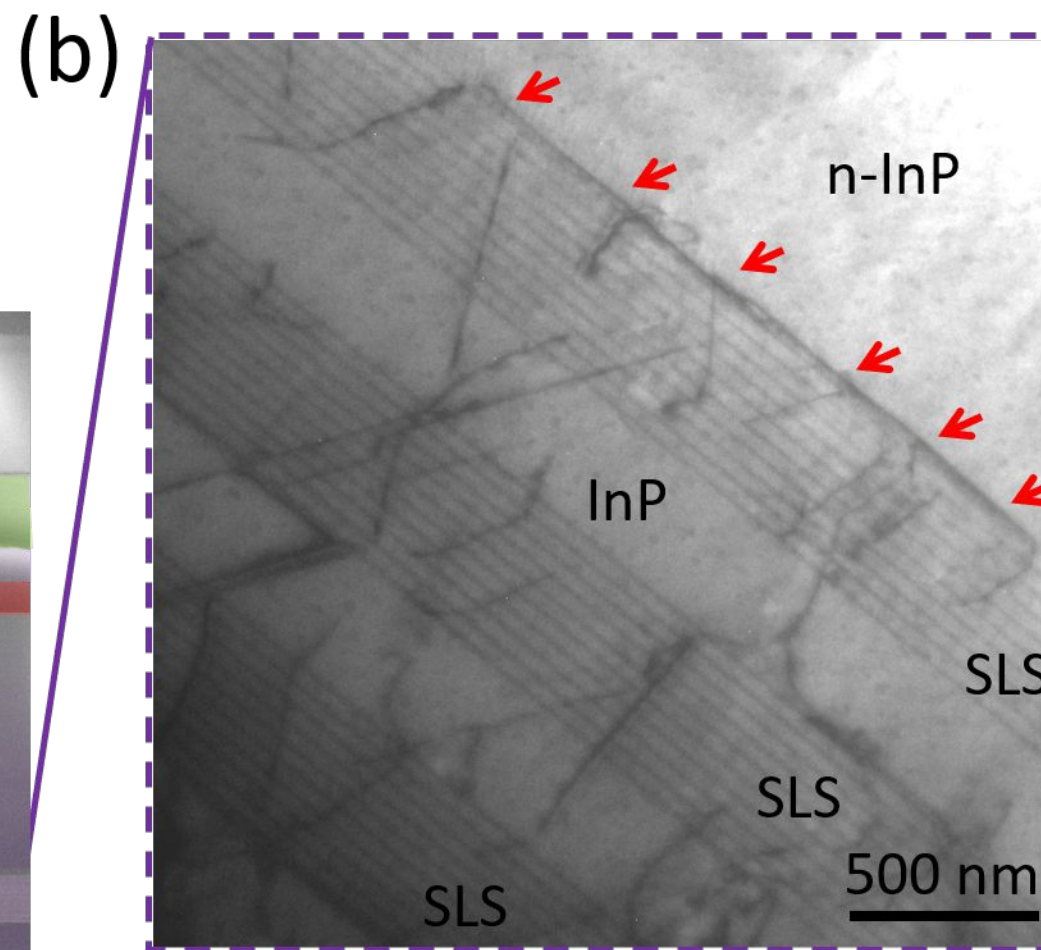
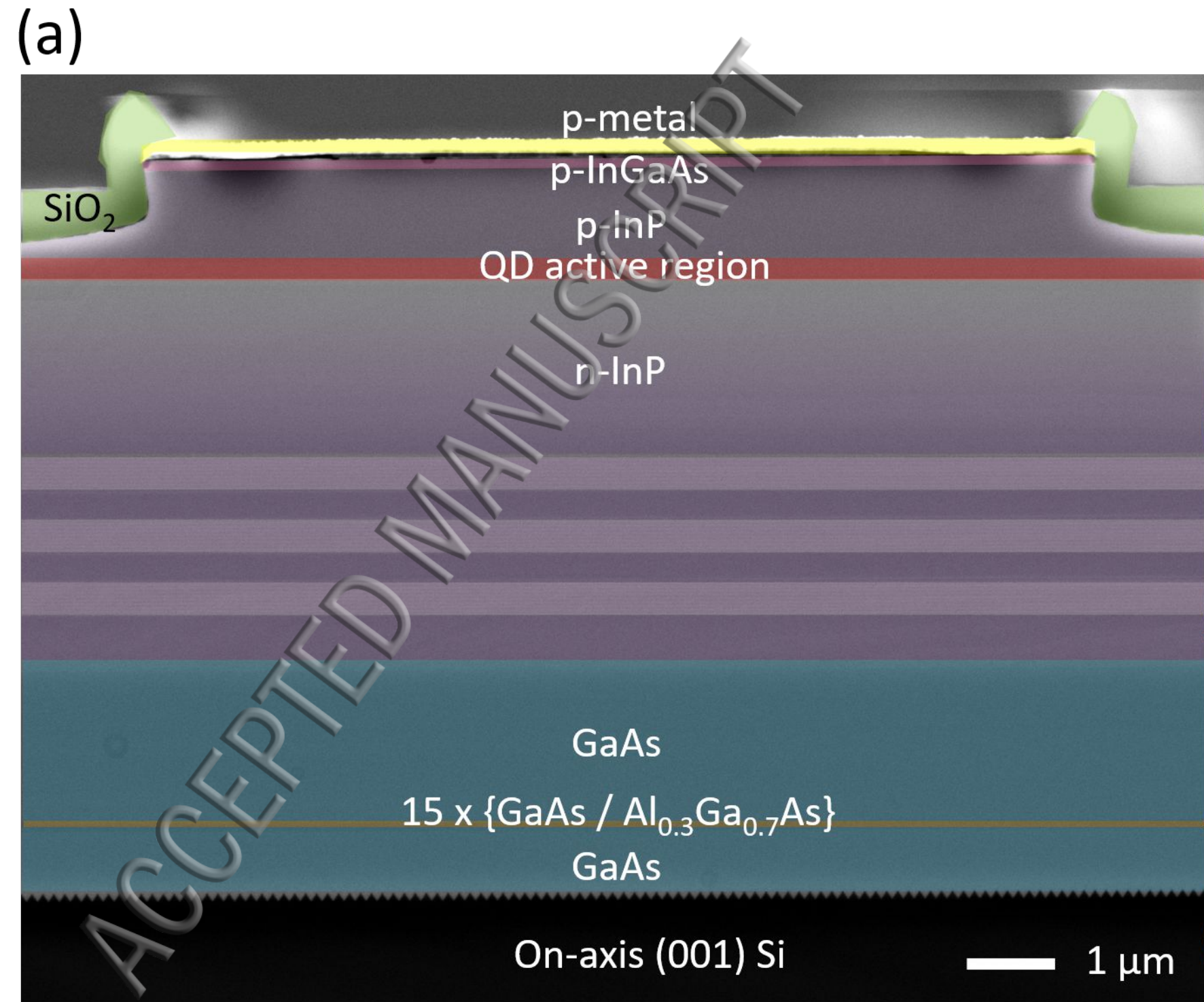
1. D. Thomson, A. Zilkie, J. E. Bowers, T. Komljenovic, G. T. Reed, L. Vivien, D. Marris-Morini, E. Cassan, L. Virost, J. Fédéli, J. M. Hartmann, J. H. Schmid, D. X. Xu, F. Boeuf, P. O'Brien, G. Z. Mashanovich, and M. Nedeljkovic, *Journal of Optics* **18**, 073003 (2016).
2. K. Yamada, T. Tsuchizawa, H. Nishi, R. Kou, T. Hiraki, K. Takeda, H. Fukuda, Y. Ishikawa, K. Wada, and T. Yamamoto, *Science and Technology of Advanced Materials* **15**, 024603 (2014).
3. T. N. Nielsen, C. Doerr, L. Chen, D. Vermeulen, S. Azemati, G. McBrien, B. Mikkelsen, C. Rasmussen, and N. Nadarajah, Engineering silicon photonics solutions for metro WDM. *Optical Fiber Communication Conference Th3J. 1* (2014).
4. A. E. Lim, T. Y. Liow, J. F. Song, M. B. Yu, C. Li, X. G. Tu, K. K. Chen, R. P. Tern, Y. Huang, X. S. Luo, G. Q. Lo, *Silicon Photonics III. Topics in Applied Physics, Springer, Berlin, Heidelberg* **122**, 191-215 (2016).
5. A. H. Atabaki, S. Moazeni, F. Pavanello, H. Gevorgyan, J. Notaros, L. Alloatti, M. T. Wade, C. Sun, S. A. Kruger, H. Meng, K. A. Qubaisi, I. Wang, B. Zhang, A. Khilo, C. V. Baiocco, M. A. Popović, V. M. Stojanović, and R. J. Ram, *Nature* **556**, 349 (2018).

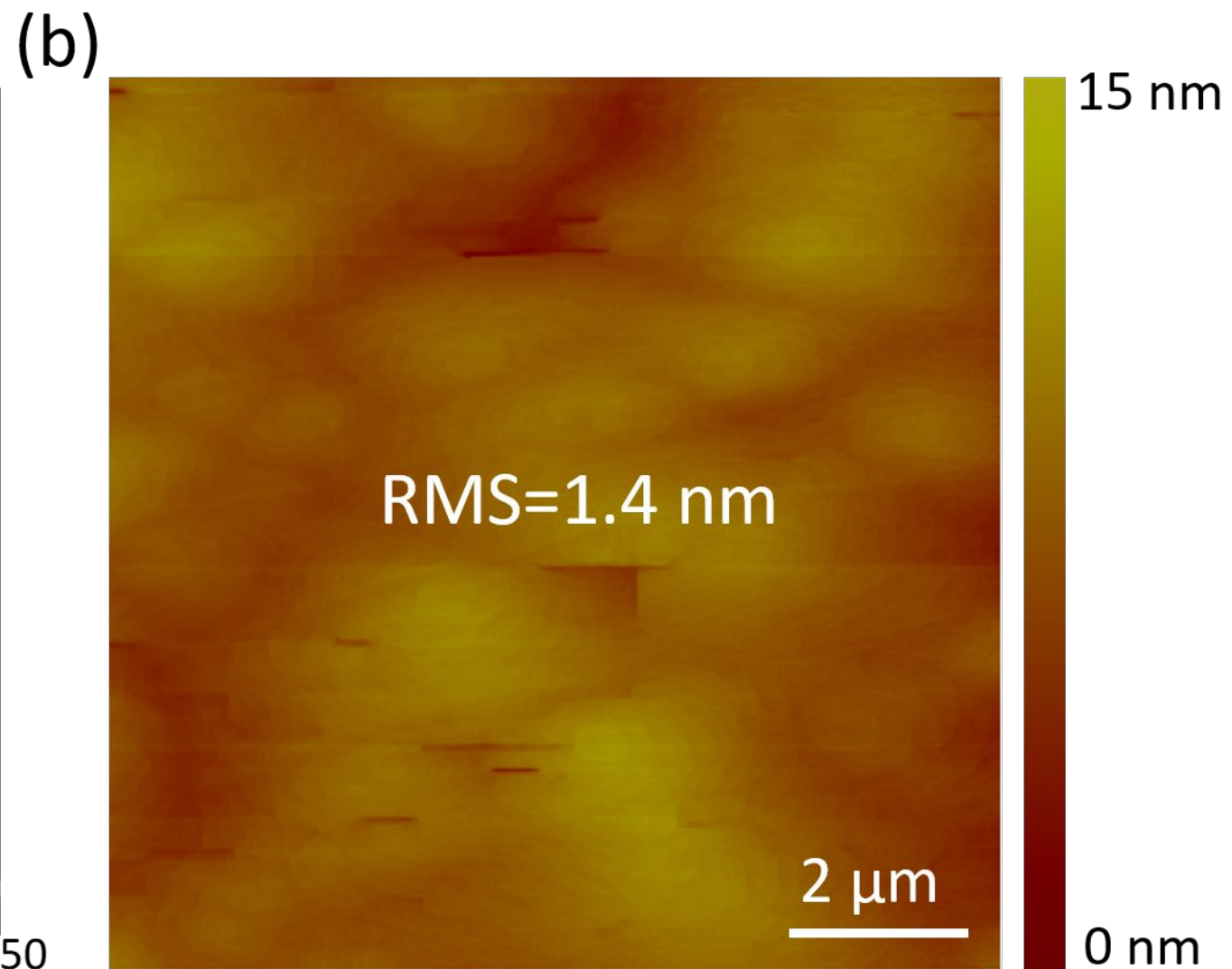
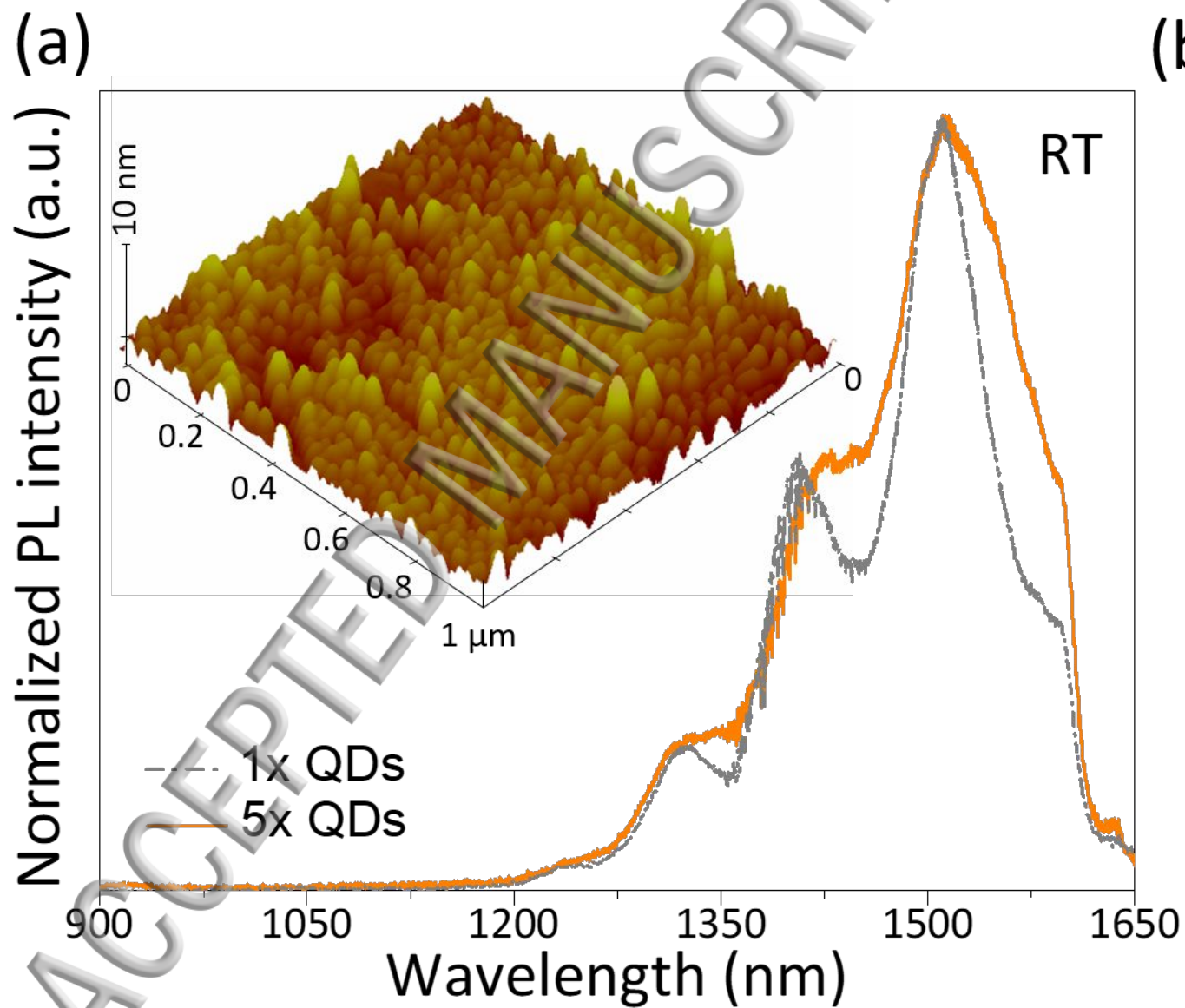
6. D. Liang, and J. E. Bowers, [Nature Photonics](#) **4**, 511 (2010).
7. J. E. Bowers, and A. Y. Liu, [Optical Fiber Communication Conference M2B](#), **4** (2017).
8. J. C. Norman, D. Jung, Y. Wan, and John E. Bowers, [APL Photonics](#) **3**, 030901 (2018).
9. S. Chen, W. Li, J. Wu, Q. Jiang, M. Tang, S. Shutts, S. N. Elliott, A. Sobiesierski, A. J. Seeds, I. Ross, P. M. Snowton, and H. Liu, [Nature Photonics](#) **10**, 307 (2016).
10. Y. Wang, S. Chen, Y. Yu, L. Zhou, L. Liu, C. Yang, M. Liao, M. Tang, Z. Liu, J. Wu, W. Li, I. Ross, A. J. Seeds, H. Liu, and S. Yu, [Optica](#) **5**, 528-533 (2018).
11. Y. Wan, J. Norman, Q. Li, M. J. Kennedy, D. Liang, C. Zhang, D. Huang, Z. Zhang, A. Y. Liu, A. Torres, D. Jung, A. C. Gossard, E. L. Hu, K. M. Lau, and J. E. Bowers, [Optica](#) **4**, 940-944 (2017).
12. P. Caroff, C. Paranthoena, C. Platz, O. Dehaese, H. Folliot, N. Bertru, C. Labbé, R. Piron, E. Homeyer, A. Le Corre, and S. Loualiche, [Appl. Phys. Lett.](#) **87**, 243107 (2005).
13. S. Bhowmick, M. Z. Baten, T. Frost, B. S. Ooi, P. Bhattacharya, [IEEE J. Quant. Electron.](#) **50**, 7-14 (2014).
14. F. I. Zubov, S. P. Gladii, Y. M. Shernyakov, M. V. Maximov, E. S. Semenova, I. V. Kulkova, K. Yvind, and A. E. Zhukov, [Journal of Physics: Conference Series](#) 012109 (2016).
15. B. Shi, S. Zhu, Q. Li, Y. Wan, E. L. Hu, and K. M. Lau, [ACS Photonics](#) **4**, 204-210 (2017).
16. S. Zhu, B. Shi, Q. Li, Y. Wan, and K. M. Lau, [Optics Express](#) **25**, 31281-31293 (2017).
17. B. Shi, S. Zhu, Q. Li, C. W. Tang, Y. Wan, E. L. Hu, and K. M. Lau, [Appl. Phys. Lett.](#) **110**, 121109 (2017).
18. A. Castellano, L. Cerutti, J. B. Rodriguez, G. Narcy, A. Garreau, F. Lelarge, and E. Tournié, [APL Photonics](#) **2**, 061301 (2017).
19. Q. Li, K. W. Ng, and K. M. Lau, [Appl. Phys. Lett.](#) **106**, 072105 (2015).

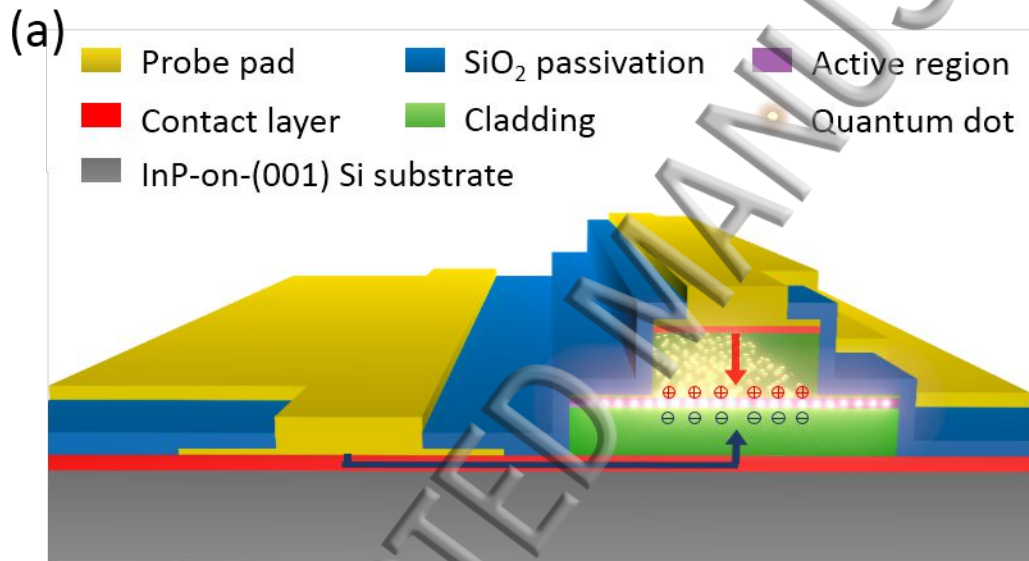
20. D. Kohen, X. S. Nguyen, R. I. Made, C. Heidelberger, K. H. Lee, K. E. K. Lee, and E. A. Fitzgerald, *J. Cryst. Growth* **478**, 64-70 (2017).
21. B. Shi, and K. M. Lau, *J. Cryst. Growth* **433**, 19-23 (2016).
22. P. J. Poole, K. Kaminska, P. Barrios, Z. Lu, and J. Liu, *J. Cryst. Growth* **311**, 1482-1486 (2009).
23. C. Paranthoen, N. Bertru, O. Dehaese, A. Le Corre, S. Loualiche, and B. Lambert, *Appl. Phys. Lett.* **78**, 1751 (2001).
24. S. Kitamura, M. Senshu, T. Katsuyama, Y. Hino, N. Ozaki, S. Ohkouchi, Y. Sugimoto, and R. A. Hogg, *Nanoscale Research Letters* **10**, 231 (2015).
25. W. Wei, J. Wang, B. Zhang, J. Zhang, H. Wang, Q. Feng, H. Xu, T. Wang, and J. Zhang, *Appl. Phys. Lett.* **113**, 053107 (2018).
26. S. Zhu, B. Shi, Q. Li, and K. M. Lau, *Optics Express* **26**, 14514-14523 (2018).
27. A. Matsumoto, K. Akahane, T. Umezawa, and N. Yamamoto, *Japanese Journal of Applied Physics* **56**, 04CH07 (2017).
28. A. Abdollahinia, S. Banyoudeh, A. Rippien, F. Schnabel, O. Eyal, I. Cestier, I. Kalifa, E. Mentovich, G. Eisenstein, and J.P. Reithmaier, *Optics Express* **26**, 6056-6066 (2018).
29. W. Rudno-Rudziński, M. Syperek, J. Andrzejewski, A. Maryński, J. Misiewicz, A. Somers, S. Höfling, J. P. Reithmaier, and G. Sęk, *AIP Advances* **7**, 015117 (2017).
30. Y. Zhang, Y. Su, Y. Bi, J. Pan, H. Yu, Y. Zhang, J. Sun, X. Sun, and M. Chong, *Opt. Lett.* **43**, 86-89 (2018).
31. M. Smit, X. Leijtens, H. Ambrosius, E. Bente, J. Tol, B. Smalbrugge, T. Vries, E. Geluk, J. Bolk, R. Veldhoven, L. Augustin, P. Thijs, D. D'Agostino, H. Rabbani, K. Lawniczuk, S. Stopinski, S. Tahvili, A. Corradi, E. Kleijn, D. Dzibrou, M. Felicetti, E. Bitincka, V. Moskalenko, J. Zhao, R. Santos, G. Gilardi, W. Yao, K. Williams, P. Stabile, P. Kuindersma,

J. Pello, S. Bhat, Y. Jiao, D. Heiss, G. Roelkens, M. Wale, P. Firth, F. Soares, N. Grote, M. Schell, H. Debregeas, M. Achouche, J. Gentner, A. Bakker, T. Korthorst, D. Gallagher, A. Dabbs, A. Melloni, F. Morichetti, D. Melati, A. Wonfor, R. Penty, R. Broeke, B. Musk, and D. Robbins, [Semiconductor Science and Technology](#) **29**, 083001 (2014).

ACCEPTED MANUSCRIPT







(Not to scale)

